Synoptic characteristics and ozone distributions associated with spring dust classes over the northern Arabian Peninsula

Abdul-Wahab S. Mashat[1] · Ahmad O. Alamoudi[1] · Adel M. Awad[1] · Mazen E. Assiri[1]

Abstract

The spring season can be classified into five dust classes over the northern Arabian Peninsula (AP), and they range from free (represented 3.3% of measured period) to strong (represented 21.4% of measured period) and were categorized based on their Total Ozone Mapping Spectrometer (TOMS) aerosol index (AI) values. The horizontal distribution of total ozone and the synoptic characteristics of these classes were analyzed using the TOMS total ozone and National Centers for Environmental Prediction (NCEP)/National Center for Atmospheric Research (NCAR) reanalysis meteorological data. The horizontal distribution of total ozone for the dust classes indicated that ozone increased (from 260 DU for dust-free to 280 DU for strong dust classes) over the southern study region. Meanwhile, the amount (from 380 DU for the dust-free to 360 DU for strong dust classes) and gradient of ozone decreased over the subtropical region as the dust class intensified, and the concentration of ozone toward the southern region was related to weak dust classes. The synoptic study indicated that the dust systems over the northern AP intensified when the atmospheric conditions were favorable for deepening the surface low pressure or a trough influenced the area and an upper-level pronounced trough and ridge occurred over the eastern and western AP. An examination of the dust cases indicated that the synoptic features that occurred with dust over the northern AP did not occur via the atmospheric systems themselves but rather via the relative relationships between these systems. Furthermore, the results confirmed that ozone over the northern (southern) AP decreased (increased) as the dust features strengthened (weakened).

Keywords TOMS total column ozone · TOMS aerosol index · Spring dust · Synoptic features · Northern Saudi Arabia

Introduction

Ozone is an important atmospheric trace gas that protects the earth from harmful radiation by absorbing incoming solar near-ultraviolet and outgoing infrared radiation from the surface.

Mineral dust is one of the greatest sources of natural aerosols and accounts for approximately 37% of the total production of atmospheric primary aerosols (i.e., 2150 Tg/year; Penner et al. 2001). These mineral aerosols strongly absorb shortwave solar radiation and reduce the photolysis rate, thereby inhibiting ozone production (Prospero et al. 1995;

✉ Adel M. Awad
awad_adel@yahoo.com; amawad@kau.edu.sa

[1] Department of Meteorology, King Abdulaziz University, P.O. Box 80208, Jeddah 21589, Saudi Arabia

Dentener and Crutzen 1993; Zhang et al. 1994; Dickerson et al. 1997). Dentener et al. (1996) studied the effect of mineral dust on ozone concentrations using a numerical model and found that ozone damage from surface-emitted mineral aerosols could lead to a 10% reduction in ozone concentrations in dust-prone areas. Additionally, the results from other studies (Fabian and Pruchniewicz 1977; Prospero et al. 1995; Schmitt and Schreiber 1998) confirmed that the air masses originating from Central Africa are accompanied by the lowest ozone concentrations. However, Soler et al. (2016) studied of 15 Saharan dust outbreaks over the mountains near the Iberian Peninsula and indicated that the reduction in ozone due to dust events was between 5 and 15%.

Bonasoni et al. (2004) performed a posterior trajectory analysis of 12 dust events that affected southern Italy to identify the main source areas of ozone and aerosols. Their statistical analysis showed that central Europe and northern and central Italy are the major pollution source areas for ozone and fine aerosols, whereas the northern African desert regions are the most important source areas for coarse aerosols

and low ozone concentrations. Additionally, Jenkins et al. (2012) studied 13 ozone readings from Cape Verde during the summer dust event of 2010 and found a negative correlation between ozone and Saharan dust.

In a global modeling study for the year 2000, Bauer et al. (2004) suggested that a global decrease in the tropospheric ozone mass by approximately 5% could be caused by heterogeneous reactions with dust aerosols.

Furthermore, Andrey et al. (2014) demonstrated that ozone in the lower troposphere is controlled by synoptic conditions, in which high ozone levels are associated with masses transported from the mid- and upper troposphere via anticyclonic systems and lower ozone concentrations are found in low-pressure systems. Singh et al. (2002) clarified the effect of El Niño on the total ozone content for most cities in India and showed that the ozone trend increased from 1996 to 2000. Moreover, Sahoo et al. (2005) reported that the total ozone content over the Indo-Gangetic basin exhibits a declining trend because of increasing pollution. Chakrabarty et al. (1998) found similar results for selected Indian cities using ground and Nimbus-7 Total Ozone Mapping Spectrometer (TOMS) data.

Varotsos et al. (2004) found a relationship between the declining amount of total column ozone and the change in the tropopause height over Athens, although this relationship has not been established over India (Sahoo et al. 2005). Smoydzin et al. (2012) investigated the influence of mesoscale patterns, summer shamal winds, and land-sea breezes on the increase in ozone over the eastern Arabian Peninsula (AP).

To further our understanding of these complex phenomena, this study analyzes the relationship between the synoptic forces that accompany the dust categories over the northern AP and the horizontal distribution of total ozone over the surrounding area.

The paper is organized as follows: The datasets used for this work are described in the "Data" section, while the employed procedures and methodology are described in the "Methodology" section. The "Results" section discusses the ozone and synoptic pattern results observed on dusty spring days and their classes, while the "Conclusions" section summarizes the main findings of the study.

Data

The TOMS instrument measures backscattered Earth radiances at six discrete ultraviolet (UV) wavelengths (312–380 nm or 308–360 nm). TOMS measures the solar irradiance for each wavelength band once a day for radiance normalization. The measured solar irradiance is recorded using a diffuser plate to scatter sunlight into the instrument, and the total ozone data are derived from the backscattered UV reflectance

via the TOMS retrieval algorithm (Antón et al. 2010). The total ozone content datasets were obtained from different TOMS instruments developed by the National Aeronautics & Space Administration (NASA)/Goddard Space Flight Center (GSFC) (ftp://toms.gsfc.nasa.gov/pub/).

The TOMS aerosol index (AI) is a semi-measured value defined as the difference between the backscattered radiation measured in two ultraviolet channels and uses a linear relationship with the optical depth due to smoke and dust (Herman et al. 1997; Torres et al. 1998). Hsu et al. (1999) performed radiative transfer calculations and showed that for a given aerosol type, the ratio AI/AOT increases with increasing altitude. The AI enables the detection of absorbing aerosols over land and water; however, it is proportional not only to the optical depth but also to the dust altitude (i.e., dust close to the surface has a relatively weak TOMS AI response, regardless of the amount of dust; Mahowald et al. 2003). However, dust near the surface produces a deficiency in AI values that can be overcome by using threshold values (Prospero et al. 2002; Washington et al. 2003; Gao and Washington 2009; Mashat et al. 2018).

A threshold AI value was applied in this study to avoid this deficiency in the measurements and was used as a criterion for the selection of dust cases. The identification method and the magnitude of this threshold value are described in the "Methodology" section. For this study, we assumed that the daily TOMS ozone and AI values were representative of 24-h periods. Data from daily global measurements of UV radiance were collected over 25 years beginning in spring 1979 and continuing until spring 2006, with a data gap from May 1993 to July 1996.

Meteorological data with a spatial resolution of 2.5° × 2.5° from NCEP/NCAR reanalysis (Kalnay et al. 1996; Kistler et al. 2001) were used to study the synoptic features of the classes and cases. These data consist of the sea-level pressures (SLPs), the wind components at pressure levels of 500 and 250 hPa, the temperatures between the pressure levels of 1000 to 500 hPa, and the geopotential height at 500 hPa during the spring months from 1979 to 2006 (i.e., March, April, and May).

Methodology

The dust cases were classified based on the selected TOMS AI threshold values. The threshold values were determined based on the average (1.381) and standard deviation (0.832) of the AI values for all cases that had at least one grid point with an AI exceeding zero within the "checking zone," which was delineated by latitudes from 26 to 32° N and longitudes from 35 to 48° E (Fig. 1a).

In their study on the influence of dust on ozone, Andrey et al. (2014) classified the cases via a simple method into clear
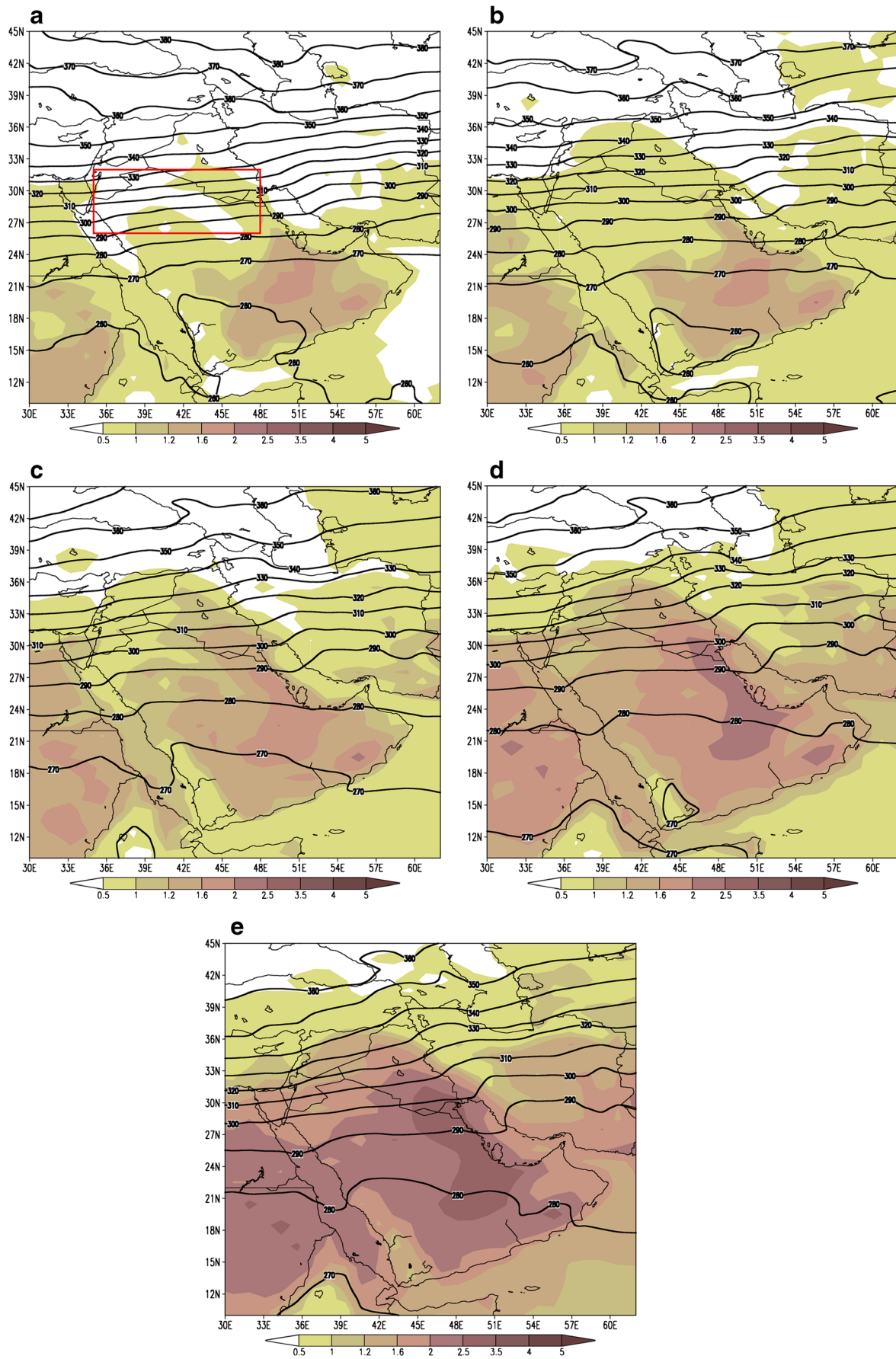
Fig. 1 Horizontal distribution of the TOMS aerosol index (dust) (shaded) and the TOMS total column ozone (contours, with a contour interval of 10 DU) for the dust classes: **a** dust-free, **b** quasi-dust, **c** weak, **d** moderate, and **e** strong

and dusty cases. The following threshold AI values were used to classify the five classes:

1. Dust-free class: all cases have AI values greater than 0 and less than the average AI value of 1.381.
2. Quasi-dust class: all cases have AI values greater than 1.381 and less than 1.797 (i.e., the average AI plus one-half the standard deviation).
3. Weak dust class: all cases have AI values greater than 1.797 and less than 2.629 (i.e., the average AI plus one and a half the standard deviation).
4. Moderate dust class: all cases have AI values greater than 2.629 and less than 3.461 (i.e., the average AI plus two and a half the standard deviation value).
5. Strong dust class: all cases have AI values greater than 3.46.

For the synoptic study, the compositions of the 12 UTC meteorological data were used for these cases because this time is closest to the TOMS observation time in the study region (i.e., approximately 11:30 local time).

Results

Class characteristics

The classification scheme outlined in the "Methodology" section was applied to the spring seasons from 1979 to 2006, and 2079 dust cases were identified. These cases represented approximately 91.6% of the spring seasons during the study period or 96.7% of the measurement period (Table 1). Moreover, over 11.2% of the measurement period was classified as quasi-dust. Most of these cases were weak to moderate dust events, which corresponded to approximately 1378 cases or 60.7% of the spring seasons, whereas only 460 cases were strong dust events, which represented approximately 20.3% of the spring seasons or 21.4% of the measurement period (Table 1).

Horizontal distribution of dust and total column ozone

Figure 1 shows the distribution of the dust amount for the different classes. The highest amount of dust in the study region for each class was proportional to the threshold value used to specify the classes. The highest amount of dust was found for the strong dust class (Fig. 1e), whereas the lowest amount of dust was found for the quasi-dust class (Fig. 1b). The visible amount of dust in the dust-free class was concentrated in the southern region of the AP (Fig. 1a), while a pronounced AI value extended over the region for the more intense dust classes.

With the lowest total ozone of 260 DU, the distribution of total ozone for the dust-free class indicated that the lowest total ozone occurred over the southwestern AP (Fig. 1a). In contrast, the highest total ozone was found over the northern region, especially over the Caspian Sea (total ozone of 380 DU). The local increase in total ozone distribution over the southern region was associated with increasing temperature (Santurtun et al. 2015) which was associated with dust. Additionally, the total ozone exhibited a strong gradient over the area between 21° N and 36° N.

Although the southwestern AP exhibited the lowest total ozone for the quasi-dust class (Fig. 1b), the total ozone over the northern region decreased to 370 DU, which was 10 DU lower than the dust-free class. Furthermore, the total ozone gradient over the study region decreased while total ozone increased over the AP and decreased to the north, which is consistent with previous results (Dentener et al. 1996; Bonasoni et al. 2004).

The horizontal distribution of total ozone for the weak dust class shown in Fig. 1c indicates that the minimum total ozone over the southern region was 270 DU and that the maximum value 370 DU was found over the northern region. Furthermore, the total ozone gradient decreased.

Figure 1d shows the results for the moderate dust class and indicates that the total ozone gradient decreased relative to that of previous classes, especially over the southern region. The minimum total ozone was 270 DU, which was 10 DU higher than the dust-free class.

For the strong dust class, the total ozone gradient decreased, especially in the southern region. However, the total ozone increased over this region (Fig. 1e) and reached 280 DU, which represented a 20 DU increase compared with the dust-free class or a 10 DU increase compared with the other classes. The total ozone decreased to 360 DU over the northern region, which is consistent with the results of Andrey et al. (2014).

In summary, previous results indicated that the increase in dust in the study region has three pronounced effects on the horizontal distribution of total ozone: increasing ozone in the southern area, decreasing ozone in the northern area, and

Table 1 Number of selected cases for each class and their percentage among the total number of selected dust cases

Classes	Free	Quasi-dust	Weak	Moderate	Strong	Total
Number of cases	72	241	780	598	460	2151
Percentage w.r.t. total number	3.3%	11.2%	36.3%	27.8%	21.4%	

decreasing the total ozone gradient over the study region, which is consistent with redistributing the total ozone in the region. However, low total ozone levels occurred near areas with a low dust level concentration over the southern region.

Synoptic study of the classes

We begin the synoptic study by describing the synoptic features of the composite of the dust-free cases and then compare these features with the synoptic features of the composites of the other dust classes to demonstrate these changes and their relationships to the strength of dust events.

SLP and the maximum wind at 250 hPa

For the dust-free class, the Siberian high, which presents a high-pressure value of 1024 hPa, has a ridge extending over the northern Mediterranean into Italy as shown in Fig. 2a. The Azores high, which has high-pressure value of 1020 hPa, has a ridge extending over the Mediterranean into Egypt. The Sudan low, which has a low-pressure value of 1008 hPa as defined by Awad and Almazroui (2016), has a strong trough over the western AP and a weak trough over the eastern AP. The Indian low has a trough over the western Arabian Gulf. The core of the maximum wind, which has a value of 99 knots, is located over the central AP near 25° N as shown in Fig. 2a.

For the quasi-dust case, SLP observations show that the Sudan low deepens to 1006 hPa, i.e., 2 hPa deeper than the dust-free class, and its trough over the eastern AP diminishes (Fig. 2b), which lifts a low over the northern Arabian Gulf, with a low-pressure value of 1012 hPa. Additionally, the Indian low deepens to 1006 hPa and merges with the Sudan low to form a low-pressure region over the southern AP, with a low-pressure value of 1010 hPa. Both the Siberian and Azores highs shrink in the eastern and western directions, respectively. Furthermore, the maximum wind, which has a value of 88 knots, weakens and shifts northward relative to the dust-free class scenario.

For the weak dust class, the low-pressure area over the southern AP deepens to 1008 hPa, i.e., 2 hPa deeper than the quasi-dust class, and a pronounced trough appears over the eastern AP (Fig. 2c). Additionally, the Sudan and Indian lows deepen to 1006 and 1004 hPa, respectively, i.e., 2 hPa deeper than the quasi-dust class. The Azores high shrinks westward and the Siberian high shrinks eastward and shifts northward. Finally, as shown in Fig. 2c, the maximum wind, which has a value of 75 knots, weakens relative to the previous class and shifts northward.

For the moderate dust class, the SLPs indicate that the low-pressure area over the southern AP deepens to 1006 hPa, i.e., 4 hPa deeper than the quasi-dust class, and both the Sudan and Indian lows form a deep trough over the northern AP and

extend northward into Turkey (Fig. 2d). Both the Azores and Siberian highs weaken, which both have a maximum pressure of 1016 hPa. Additionally, the Azores high shrinks westward while the Siberian high shifts northward relative to the previous classes. The shrinking of the Azores and Siberian high systems around the northern AP produced the favor conditions for the northward extension of the southern AP low-pressure system (Baseer et al. 2019). Figure 2d shows that the maximum wind, which has a value of 69 knots, weakens and shifts northward relative to the previous classes.

For the strong dust class, the SLPs indicate that the southern AP low-pressure area present in the previous classes becomes part of the Indian low, with a low-pressure value of 1006 hPa, as shown in Fig. 2e. A deep trough over the eastern AP forms from the deepened Sudan and Indian low-pressure systems. Furthermore, the Azores and Siberian highs shrink and shift northward, while the maximum wind, with value 67 knots, weakens and shifts northward relative to the previous classes.

The atmospheric features accompanying different classes demonstrated that the low-pressure systems deepen and extend northward, the high-pressure systems shrink away from the northern AP, and the jet stream weakens and shifts northward as the dust increased.

Synoptic features at 500 hPa and the static stability between 1000 and 500 hPa

The atmospheric state for the dust-free class (Fig. 3a) demonstrates a deep cyclonic region over the northern AP, with a low height of 5360 gpm, and a flat trough was present over the Red Sea and the AP. Furthermore, a ridge from the southern anticyclone, with a highest value of 5850 gpm, influences the eastern AP and Iran. The distribution of static stability (Fig. 3a) shows high stability over the study area, especially over the northeast and southeast regions, which have values of 1.0 deg db^{-1} and 1.05 deg db^{-1}, respectively. However, relatively low stability areas are located over the southwestern and northern AP, which have a value of 0.5 deg db^{-1}.

The atmospheric features for the quasi-dust class (Fig. 3b) indicate a weakening northern cyclone, with a low height of 5430 gpm. However, a pronounced trough over the Red Sea and a weak ridge from the southern anticyclonic system affect the AP, with a high value of 5830 gpm. Furthermore, compared with the dust-free class, the horizontal distribution of static stability shows a decrease in stability across the entire AP region (Fig. 3b), where the low value is 0.45 deg db^{-1} over the northern AP. The main feature distinguishing the quasi-dust class from the dust-free class is the improved atmospheric mechanisms, which lead to a pronounced trough over the Red Sea, a weakened ridge from the southern anticyclone and decreased stability.
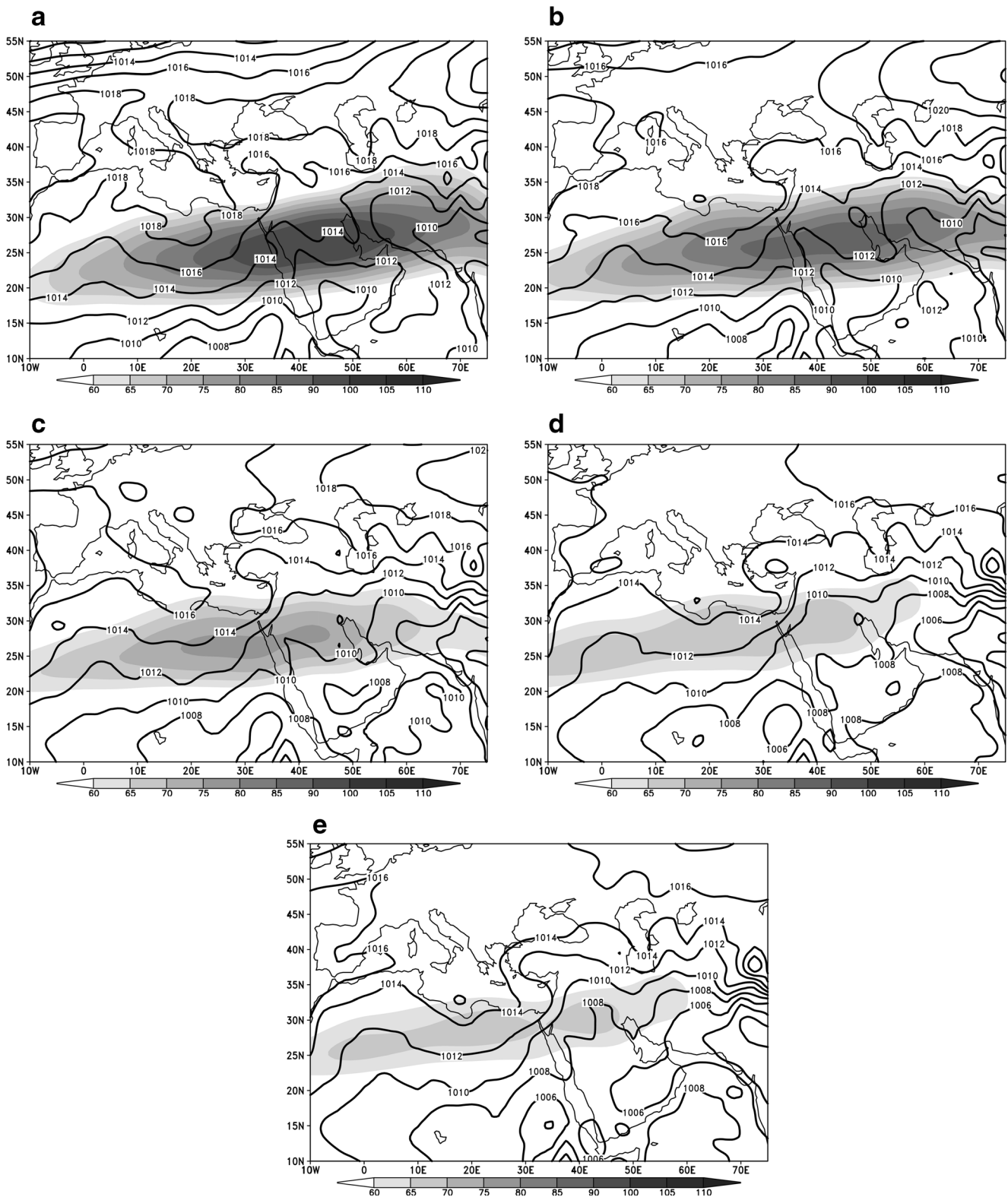
Fig. 2 Mean sea level pressure (SLP) in hPa (contours) and the maximum winds at 250 hPa in knots (shaded) for the dust classes: **a** dust-free, **b** quasi-dust, **c** weak, **d** moderate, and **e** strong

For the weak dust class (Fig. 3c), the northern cyclone weakens further, the lowest height is 5490 gpm, and both the trough over the Red Sea and the ridge over the AP become more pronounced. Additionally, a core from the subtropical anticyclone appears over Africa, with a highest value of 5880 gpm. As in the previous class, the
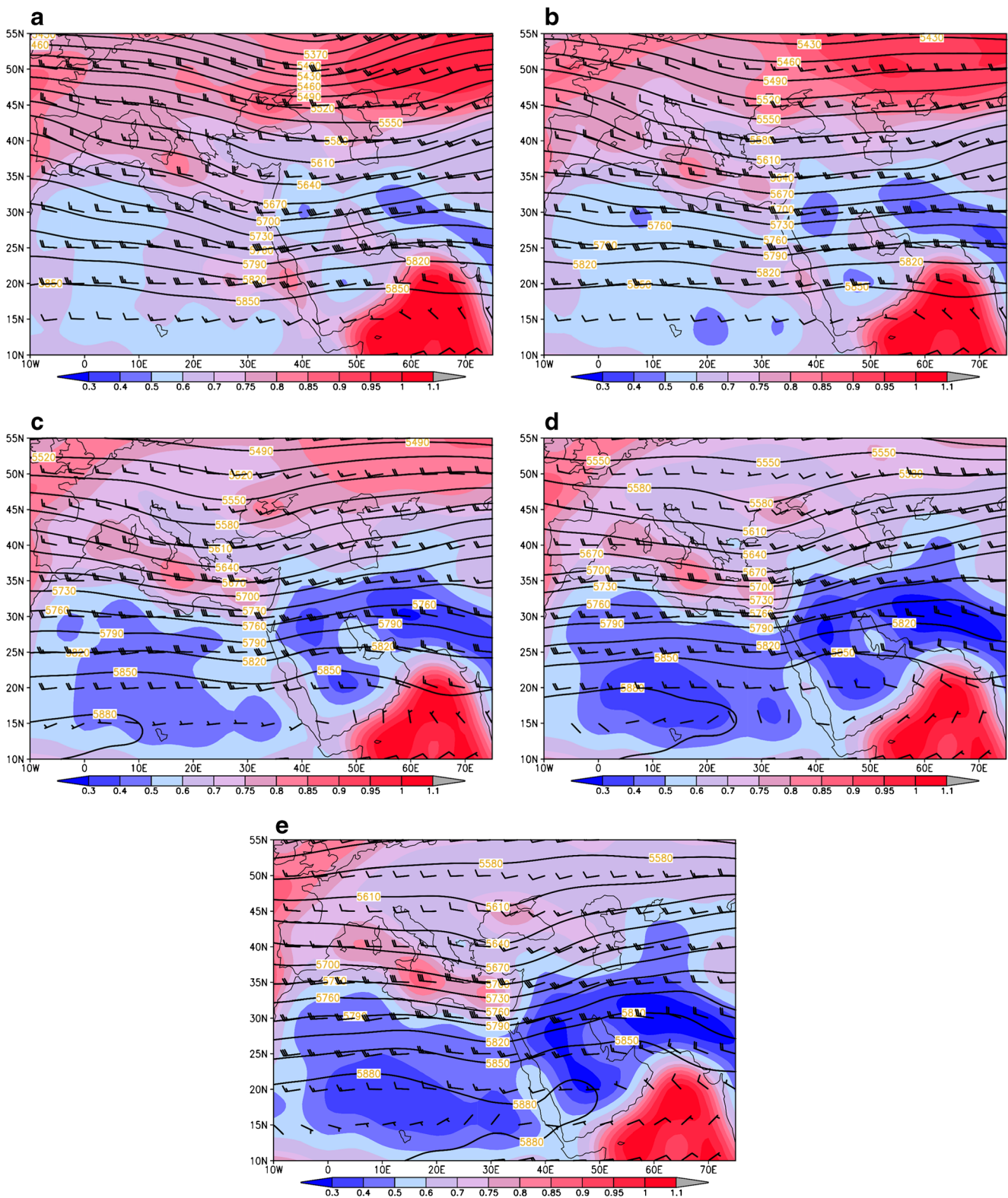
Fig. 3 Geopotential height (in gpm) and wind vectors (contours and barbs, respectively) at 500 hPa and the static stability between 1000 and 500 hPa (shaded) for the dust classes: **a** dust-free, **b** quasi-dust, **c** weak, **d** moderate, and **e** strong

static stability continues to decrease in the study area, especially over the AP and Africa (Fig. 3c), where the stability reached 0.4 deg db^{-1} and 0.5 deg db^{-1}, respectively. Obviously, the mechanisms underlying the generation of the quasi-dust class in the atmosphere continue to improve in this class.

For the moderate dust class (Fig. 3d), the weakening of the northern cyclone continues, the lowest height is 5550 gpm, the geopotential height increases by 210 gpm relative to that of the dust-free composite, and the ridge over the AP becomes more pronounced as the core subtropical anticyclone extends eastward to east Africa. As with the previous classes, the static stability continues to decrease (Fig. 3d) and the Mediterranean exhibits high stability, which has a value of 0.8 deg db^{-1}, whereas the areas from Iran to India and over the AP have low stability, which have values of 0.3 deg db^{-1} and 0.35 deg db^{-1}, respectively.

The atmospheric systems for the strong dust class (Fig. 3e) indicate that the northern cyclone becomes very weak and the lowest height is 5580 gpm, which represents an increase of 240 gpm relative to that in the dust-free composite. The subtropical high, which has a high value of 5880 gpm, extends eastward to the southern AP and forms a pronounced ridge over the eastern AP. Additionally, despite the horizontal distribution of stability shown in Fig. 3e, which is similar to that of the moderate dust class, the area of low stability over the AP, which has a value of 0.3 deg db^{-1}, becomes elongated.

The previous description demonstrated that the stability decreased and the atmospheric systems, namely, troughs and ridges, and their interactions were pronounced as the dust increased.

Case study

This section examines five case studies, with one for each class. The corresponding horizontal dust and ozone distribution are compared with the results for each class. In addition, the synoptic characteristics of the cases are examined, and their relationship with dust and ozone are discussed.

Horizontal distribution of dust and total column ozone

For the dust-free case on 13 March 2005 (Fig. 4a), the dust concentrated over the *southwestern* region and low amounts were observed over the northern region. The horizontal distribution of total ozone exhibited a pronounced gradient between 24° N and 36° N. Furthermore, the distribution showed that the lowest total ozone was approximately 240 DU in the southern region and the highest value was 420 DU over the northeastern region.

For the quasi-dust case on 14 March 2005 (Fig. 4b), the majority of the dust appeared in the southern region while relatively little dust affected the northern region. The largest amount of dust over the checking zone appeared over the southwestern area. The horizontal distribution of total ozone (Fig. 4b) indicated that the lowest total ozone of 260 DU was located over the southern region while the highest total ozone of 400 DU was located over the northern region. Thus,

compared with the dust-free case, the lowest ozone value increased by 20 DU and the highest value decreased by 20 DU. Furthermore, a high total ozone gradient was concentrated over the zonal area between 24° N and 33° N. The ozone distribution accompanying this case indicated the redistribution of ozone, which increased to the south, decreased to the north, and reduced the ozone gradient compared with the ozone gradient of the dust-free case.

For the weak dust case on 8 March 2003 (Fig. 4c), most of the dust was concentrated in the southern region and extended northward into Jordan and Iraq, whereas the lowest amount occurred in the northern region. Compared with the previous cases, the horizontal distribution of total ozone (Fig. 4c) indicated a weak gradient over the region between 24° N and 36° N. Furthermore, the data indicated that the lowest total ozone of 260 DU occurred over the southern region while the highest level of 360 DU occurred over the northern region. Thus, compared with the dust-free case, *the highest value decreased by 60 DU*. Similar to the previous case, the total ozone redistributed and the gradient over the Middle East decreased as the amount of dust increased.

For the moderate dust case on 3 April 2005 (Fig. 4d), the dust increased over the southern AP and extended northward into Syria and Iraq. The maximum amount of dust in the checking zone occurred in the south-central portion of the area. Moreover, Fig. 4d shows that the lowest total ozone value of 260 DU occurred in the southern region while the highest value of 400 DU was found along the Mediterranean coast of Turkey. Thus, compared with the dust-free case, the highest value decreased by 20 DU and shifted southward. Additionally, compared with the analogous 320 DU isoline for the previous case, the peak ozone area shifted northward over the AP and strengthened over the area between 24° N and 42° N. Although the highest total ozone shifted to over the Mediterranean, the total ozone increased over the northern AP, which indicated the decrease in ozone gradient.

For the strong dust case on 5 April 2004 (Fig. 4e), the highest dust amounts were found over the mid-AP and the dust spread over the entire study area. The distribution of total ozone (Fig. 4e) indicated that the lowest total ozone of 260 DU occurred in the south while the highest total ozone of 420 DU occurred in the northern region. These results indicate that the peak ozone area shifted northward compared to the analogous 320 DU isolines from the previous cases. Finally, the strong gradient area of total ozone shifted northward toward 27° N and 45° N.

Generally, the total ozone distribution is similar between the selected cases and the corresponding classes, where the lowest value was found in the southern region and the highest value was found in the northern region. In addition, the strongest gradient area of total ozone shifted northward as the strength of the dust classes intensified.
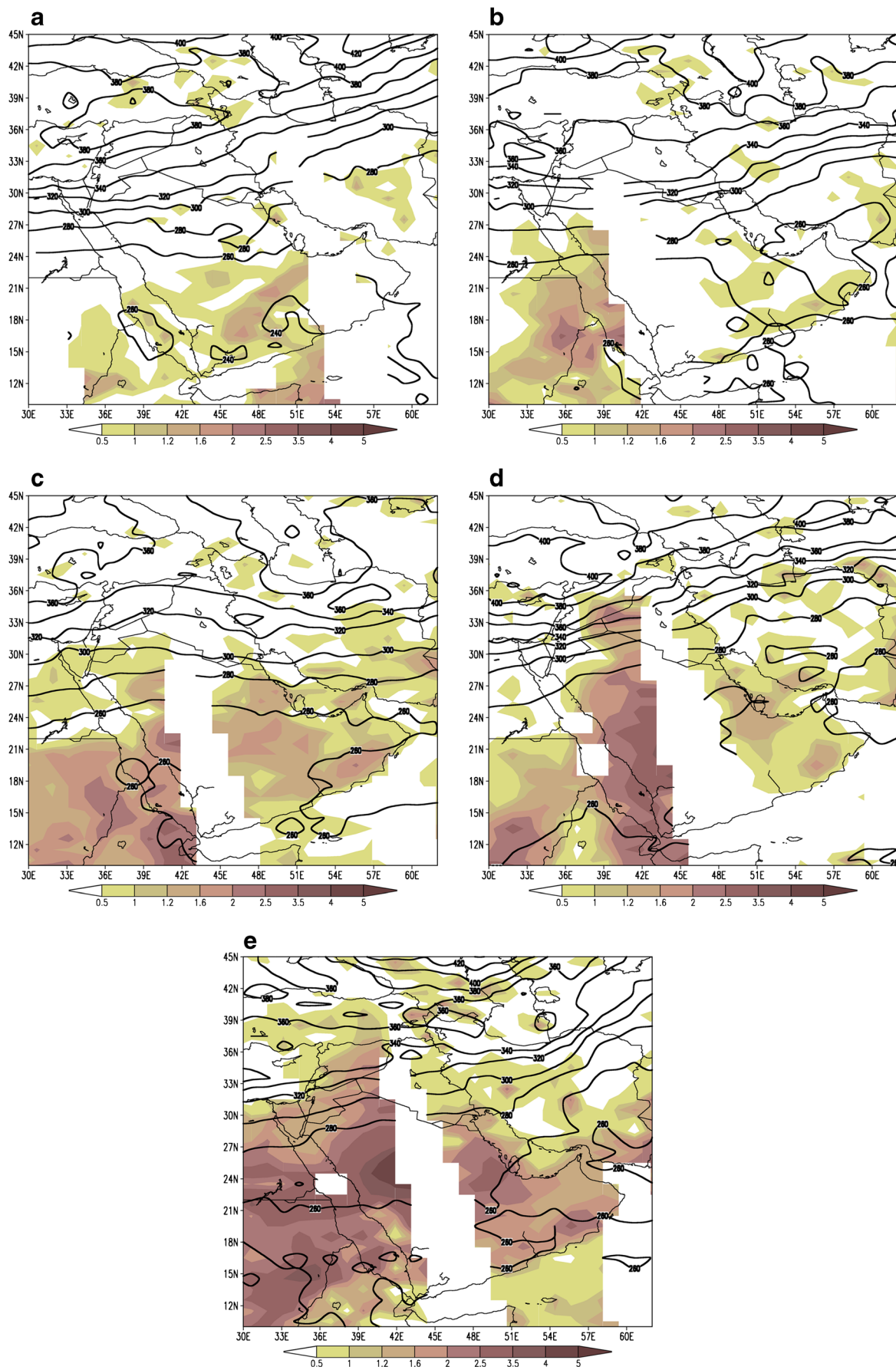
Fig. 4 Horizontal distribution of the TOMS aerosol index (dust) (shaded) and the TOMS total column ozone (contours, with a contour interval of 10 DU) for the dust cases: **a** 12 March 2005, **b** 14 March 2005, **c** 8 March 2003, **d** 3 April 2005, and **e** 5 April 2004

SLP and maximum wind at 250 hPa

The atmospheric system accompanying the dust-free case (Fig. 5a) contains two high-pressure systems, with one occurring over the eastern Mediterranean and presenting a high-pressure value of 1024 hPa and the other occurring over the northern AP and presenting a high-pressure value of 1020 hPa. These two high-pressure systems form two ridges over eastern Africa and the eastern AP. A low-pressure area, with a low-pressure value of 1008 hPa, is located over the southern AP and forms a trough over the western AP between the two ridges. The maximum wind (Fig. 5a) exhibits a core of strong winds over northern Libya, Egypt, and the western AP, and it has a value of 126 knots.

Regarding the quasi-dust case (Fig. 5b), the two high-pressure areas shown in the previous case merge to form a single high-pressure area located over Romania and the Black Sea, and it has a high-pressure value of 1024 hPa. Thus, the high-pressure systems shift northward relative to the dust-free case. However, this new high-pressure system retains the two ridges: a deep one over eastern Africa and a weak one over the eastern AP. In addition, the low-pressure area over the southern AP, with a value of 1008 hPa, forms a trough over the western AP and becomes deeper and wider relative to the previous case. The maximum wind (Fig. 5b) exhibits two strong wind core branches: one occurs over the western Red Sea and has a value of 122 knots and the other one occurs over the eastern Arabian Gulf and has a value of 142 knots. Relative to the previous case, these two branches have stronger winds and form a trough of high winds over the northern AP.

For the weak dust case (Fig. 5c), a ridge from the northern high-pressure system, which has a high-pressure value of 1034 hPa, influences the eastern AP, and the trough from the Sudan low, which has a value of 1004 hPa, affects the Red Sea by the Red Sea trough (RST) (Tsvieli and Zangvil 2005; Krichak et al. 2012; Awad and Almazroui 2016; Baseer et al. 2019). Moreover, a core of high winds, which has a value of 134 knots over eastern Arabian Gulf, forms over the northern AP.

In the moderate dust case (Fig. 5d), eastern Africa is influenced by a high-pressure ridge located over southern Europe, which has a high-pressure value of 1030 hPa. Furthermore, the Sudan low, which has a low-pressure value of 1004 hPa, merges with the low-pressure area over the southern AP, which has a low-pressure value of 1008 hPa, and forms a trough over the northeastern AP. Moreover, the maximum wind, which has a value of 186 knots over the eastern Arabian Gulf (Fig. 5d), forms a core area over the Levant area that is stronger and further northward of the core compared to the previous case. The highest total ozone and the core of the high-pressure system affect the area, thus emphasizing the

findings of Tang et al. (2009), who showed that high ozone accompanies high-pressure systems.

For the strong dust case, Fig. 5e shows that a ridge extending from a high-pressure area over Turkey, which has a high-pressure value of 1022 hPa, influences the eastern AP. Moreover, a trough from the low-pressure area, with a low-pressure value of 1006 hPa located over the southern AP, affected the western AP and the Red Sea. Finally, the maximum wind, which has a value of 237 knots over the eastern Arabian Gulf, formed a ridge shape over the northern AP, with the highest winds occurring over Iraq.

Based on the results of Awad and Mashat (2016) and the results presented herein for the various classes and cases, the maximum wind in the strong dust classes exhibits large north-south variability, indicating that many synoptic features accompany dust systems and affect the northern AP dust cases.

Synoptic features at 500 hPa and static stability between 1000 and 500 hPa

The synoptic features for the dust-free case (Fig. 6a) indicated that the northern cyclone, with a low height value of 5190 gpm, exhibits a wide trough across the eastern Red Sea. Furthermore, a subtropical anticyclone, with a high height value of 5880 gpm, influences the southern region. The horizontal distribution of the static stability (Fig. 6a) indicates that three areas of high stability over the northeastern AP, Egypt, and Arabian Sea have values of 1.1 deg db^{-1}, 1.0 deg db^{-1}, and 1.1 deg db^{-1}, respectively, and surround two areas of low stability over the southern and northwestern AP, which have values of 0.4 deg db^{-1} and 0.6 deg db^{-1}, respectively.

For the quasi-dust case (Fig. 6b), the northern cyclone, with a low height value of 5280 gpm, exhibits a deep trough over the AP, while the southern region is affected by the subtropical anticyclone, with a high height value of 5880 gpm. Additionally, the distribution of the static stability (Fig. 6b) indicates that the low stability (0.6 deg db^{-1}) over the northwestern AP, which was also observed in the previous case, increases in strength and becomes elongated because of the low stability area over Iran (0.4 deg db^{-1}). The cases study clearly confirmed that the atmospheric mechanisms improved the dust cases as demonstrated in the classes.

For the weak dust case (Fig. 6c), the center of the northern cyclone, with a low height value of 5430 gpm, shifts southward over the northern Black Sea and has a deep trough over Egypt. The subtropical anticyclone over the southern Red Sea, with a value of 5880 gpm, forms a ridge over the AP. The distribution of static stability (Fig. 6c) indicates that a decrease occurs in the high static stability (0.8 deg db^{-1}) over the northeastern AP, which is also observed in the previous case, whereas a shift to low stability (0.5 deg db^{-1}) occurs over the western and southern AP. The atmospheric features of this
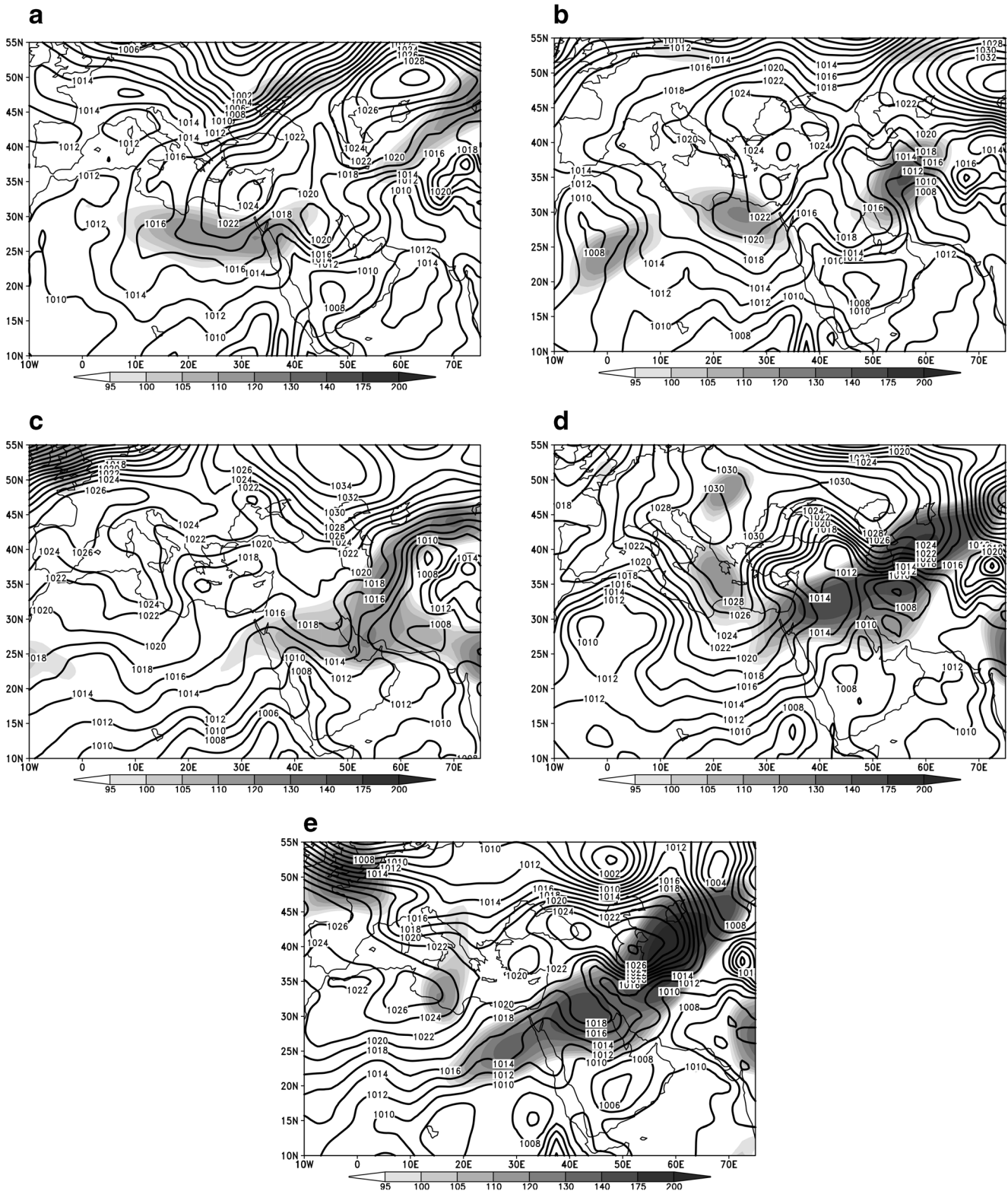
Fig. 5 Mean sea level pressure in hPa (contours) and the maximum winds at 250 hPa in knots (shaded) for the dust cases: **a** 12 March 2005, **b** 14 March 2005, **c** 8 March 2003, **d** 3 April 2005, and **e** 5 April 2004

case show that the southward shift of the northern cyclone increased the depth of the upper trough, which enhanced the atmospheric mechanisms mentioned for the classes.

Regarding the moderate dust case (Fig. 6d), the center of the northern cyclone, with a low height value of 5520 gpm, shifts south of the Black Sea and has a wide trough over the
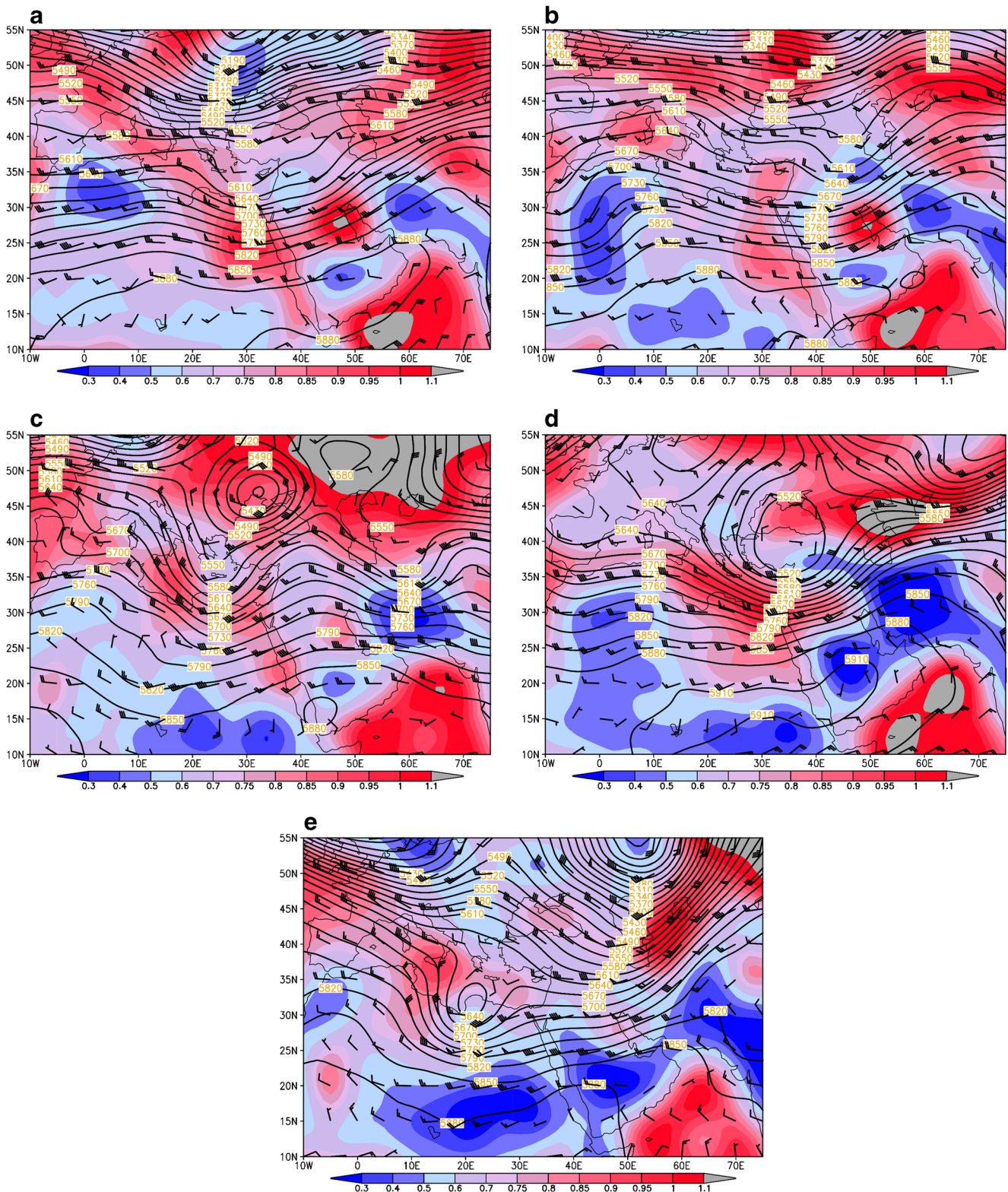
Fig. 6 Geopotential height (in gpm) and wind vectors (contours and barbs, respectively) at 500 hPa and the static stability between 1000 and 500 hPa (shaded) for the dust classes: **a** 12 March 2005, **b** 14 March 2005, **c** 8 March 2003, **d** 3 April 2005, and **e** 5 April 2004

Red Sea. Furthermore, the subtropical anticyclone in the southern region, with a high height value of 5910 gpm, forms a ridge over Iran. The distribution of stability (Fig. 6d) indicates that the majority of the AP exhibits low stability (0.2 deg db^{-1}), whereas the northern region is influenced by relatively high stability (0.8 deg db^{-1}) extending from the high

stability region over northern Egypt (1.0 deg db^{-1}). Finally, the low stability over the AP (0.2 deg db^{-1}) is related to the low stability area over Iran.

Two cyclonic systems influence the study area in the strong dust case as shown in Fig. 6e. One of these systems is located over northern Libya, with a low height value of 5640 gpm, and forms a deep trough over Libya and western Egypt, and the other system is located over the northeast region, with a low height value of 5130 gpm, and has a wide trough over the eastern AP. The subtropical anticyclone over the southern region, with a high height value of 5880 gpm, forms a weak ridge over the Red Sea. Furthermore, the stability distribution in this case (Fig. 6e) indicates that the southern AP has very low stability (0.2 deg db^{-1}) that is connected to the low stability area over Africa (0.3 deg db^{-1}), whereas the northeastern AP is influenced by relatively high stability.

Conclusions

This study examined the ozone and synoptic features associated with different classes of dust affecting the northern AP. Five distinct dust cases were classified based on the TOMS AI threshold values. The TOMS AI data within the checking zone (delineated by 26° N to 32° N and 35° E to 48° E) were used to determine these threshold values.

The threshold values were applied to all spring seasons from 1979 to 2006, and the results showed that the northern AP is affected by dust for most of the spring seasons, i.e., approximately 85.5% of the time. However, most dust cases can be categorized as weak or moderate, which represent approximately 64.1% of the investigated cases, whereas only approximately 21.4% of the total number of cases belong to the strong dust case category.

For the different classes, the horizontal distribution of dust indicated that the dust amount and dust spread area increased as the intensity of the dust class increased over the entire study area, which indicates that the intensity of dust over the northern AP may be used as a remote sensing indicator of dust intensity over the whole AP. Moreover, the horizontal distribution of total ozone for these classes demonstrated that the ozone horizontal gradient decreased and the total ozone increased in the southern AP region but decreased in the northern AP region as the dust increased. Moreover, the difference between the minimum and maximum total ozone decreased for the more severe dust categories. Rodríguez et al. (2009) estimated a reduction in ozone of 40% under dusty conditions in their study.

The SLPs indicated that the trough over the eastern regions, the low-pressure area over the southern AP, and both the Sudan and Indian low-pressure systems deepened as the dust classes intensified. However, the Azores and Siberian high-pressure systems weakened and the composite maximum wind at 250 hPa weakened and shifted northward as the dust classes intensified.

Previous synoptic features enhanced the unstable atmospheric conditions and produced favorable conditions for the stronger dispersion and/or dilution of ozone, especially in the lower atmospheric layer (Tang et al. 2009), and the dispersion and intensification of dust over the region.

Additionally, the atmospheric features at 500 hPa indicated that the northern cyclone weakened and the subtropical anticyclone strengthened as the dust class intensified. Moreover, the structure of the atmosphere showed that while the system exhibited a flat trough over the Red Sea and the AP in the dust-free class, the atmosphere transformed into two pronounced systems: a trough over the Red Sea and a ridge over the eastern AP for the most severe dust class. These features accompanying the severe dust cases increased the geopotential gradient and increased the dynamical lifting mechanisms in the atmosphere.

Furthermore, the horizontal distribution of the static stability between 1000 and 500 hPa suggested that the stability over the AP decreased as the dust class intensified, although it increased over the Mediterranean region.

An examination of the dust cases demonstrated that the horizontal distribution of total ozone exhibits little variability for the strong dust case, especially in the subtropical region, and the total ozone decreased northward as the dust cases intensified.

The synoptic features of the dust cases at the mean SLP indicated that the dust increased and that the ozone decreased over the northern AP when the high-pressure area or ridge over the northern AP weakened (in a relative sense) compared with the change of intensity of the low-pressure area or trough over the AP. In addition, the maximum wind at a pressure level of 250 hPa increased as the dust case intensified and generated a trough shape over the northern AP. A comparison of the maximum wind features of the case studies and the class compositions indicated that the maximum wind accompanying strong dust cases shifted from north to south from case to case but primarily intensified and shifted northward.

Furthermore, the synoptic features of the dust cases at 500 hPa demonstrated that the dust increased and ozone decreased over the northern AP when the synoptic conditions weakened, i.e., a weak trough or ridge. Additionally, the static stability distribution over the AP and surrounding area indicated that dust increased and ozone decreased over the northern AP as the stability over the AP and surrounding areas decreased.

References

Andrey J, Cuevas E, Parrondo MC, Alonso-Pérez S, Redondas A, Gil-Ojeda M (2014) Quantification of ozone reductions within the Saharan air layer through a 13-years climatologic analysis of ozone profiles. Atmos Environ 84:28–34

Antón M, Koukouli ME, Kroon M, McPeters RD, Labow GJ, Balis D, Serrano A (2010) Global validation of empirically corrected EP-Total Ozone Mapping Spectrometer (TOMS) total ozone columns using Brewer and Dobson ground-based measurements. J Geophys Res 115:D19305. https://doi.org/10.1029/2010JD014178

Awad AM, Almazroui M (2016) Climatology of the winter Red Sea trough. Atmos Res 182:20–29. https://doi.org/10.1016/j.atmosres.2016.07.019

Awad AM, Mashat AS (2016) Synoptic characteristics of spring dust days over northern Saudi Arabia. Air Qual Atmos Health 9:41–50. https://doi.org/10.1007/s11869-015-0320-0

Baseer NM, Awad AM, Almazroui M (2019, 2019) Climatology of the spring Red Sea trough. Int J Climatol:1–16. https://doi.org/10.1002/joc.6069

Bauer SE, Balkanski Y, Schulz M, Hauglustaine DA, Dentener F (2004) Global modeling of heterogeneous chemistry on mineral aerosol surfaces: influence on tropospheric ozone chemistry and comparison to observations. J Geophys Res 109:D02304. https://doi.org/10.1029/2003JD003868

Bonasoni P, Cristofanelli P, Calzolari F, Bonaf U, Evangelisti F, Stohl A, Zauli SS, van Dingenen R, Colombo T, Balkanski Y (2004) Aerosol-ozone correlation during dust transport episodes. Atmos Chem Phys 4:1201–1215

Chakrabarty DK, Peshin SK, Pandya KV, Shah NC (1998) Long-term trend of ozone column over the Indian region. J Geophys Res 103: 19 245–19 251

Dentener FJ, Crutzen P (1993) Reaction of N2O5 on tropospheric aerosol: impact on the global distributions of NOx, O3 and OH. J Geophys Res 98:7149–7163

Dentener FJ, Carmichael GR, Zhang Y, Lelieveld J, Crutzen PJ (1996) The role of mineral aerosols as a reactive surface in the global troposphere. J Geophys Res. 101:22 869–22 889

Dickerson RR, Kondragunta S, Stenchikov G, Civerolo KL, Doddrige BG, Holben BN (1997) The impact of aerosols on solar ultraviolet radiation and photochemical smog. Science 278:827–830

Fabian P, Pruchniewicz PG (1977) Meridional distribution of ozone in the troposphere and its seasonal variations. J Geophys Res 82:2063–2073

Gao H, Washington R (2009) The spatial and temporal characteristics of TOMS AI over the Tarim Basin, China. Atmospheric Environment 43(5):1106–1115 https://doi.org/10.1016/j.atmosenv.2008.11.013S

Herman JR, Bhartia P K, Torres O, Hsu C, Seftor C, Celarier E (1997) Global distribution of UV-absorbing aerosols from Nimbus-7/TOMS data. J GeophysRes 102:16911–16922

Hsu NC, Herman JR, Torres O, Holben BN, Tanre D, Eck TF, Smirnov A, Chatenet B, Lavenu F (1999) Comparisons of the TOMS aerosol index with Sun photometer aerosol optical thickness: Results and applications. J Geophys Res. 104:6269–6279

Jenkins G, Robjhon M, Smith J, Clark J, Mendes L (2012) The influence of the SAL and lightning on tropospheric ozone variability over the northern tropical Atlantic: results from Cape Verde during 2010. Geophys Res Lett 39:L20810

Kalnay E, Kanamitsu M, Kistler R, Collins W, Deaven D, Gandin L, Iridell M, Saha S, White G, Woollen J, Zhu Y, Chelliah M, Ebisuzaki W, Higgins W, Janowiak J, Mo KC, Ropolewski C, Wang J, Leetma A, Reynolds R, Jenne R, Joseph D (1996) The NCEP/NCAR 40-year Reanalysis project. Bull Am MeteorolSoc 77: 437–471

Kistler R, Collins W, Saha S, White G, Woollen J, Kalnay E, Chelliah M, Ebisuzaki W, Kanamitsu M, Kousky V, vandenDool H, Jenne R, Fiorino M (2001) The NCEP/NCAR 50-year Reanalyses: Monthly CD-ROM and documentation. Bull Am MeteorolSoc 82:247–267

Krichak SO, Breitgand JS, Feldstein SB (2012) A conceptual model for the identification of active Red Sea trough synoptic events over the Southeastern Mediterranean. J Appl Meteor Climatol 51:962–971. https://doi.org/10.1175/JAMC-D-11-0223.1

Mahowald NM, Luo C, delCorralJ, Zender C (2003) Interannual variability in atmospheric mineral aerosols from a 22-year model simulation and observation data. J Geophys Res 108 (D12). https://doi.org/10.1029/2002JD002821

Mashat A-WS, Alamoudi AO, Awad AM, Assiri ME (2018) Seasonal variability and synoptic characteristics of dust cases over southwestern Saudi Arabia. Int J Climatol 38:105–124. https://doi.org/10.1002/joc.5164

Penner JE, Andreae M, Annegarn H, Barrie L, Feichter J, Hegg D, Jayaraman A, Leaitch R, Murphy D, Nganga J, Pitari G (2001) In: Houghton JT, Ding Y, Griggs DJ, Noguer M, van der Linden PJ, Dai X, Maskell K, Johnson CA (eds) Aerosols, their Direct and Indirect Effects, Climate Change 2001: the Scientific basis, Contribution of Working Group 1 to the Third Assessment Report of Intergovernmental Panel on Climate Change, vol 881. Cambridge Univ. Press, Cambridge

Prospero JM, Ginoux P, Torres O, Nicholson SE, Gill TE (2002) Environmental characterization of global sources of atmospheric soil dust identified with the Nimbus 7 total ozone mapping spectrometer absorbing aerosol product. Reviews of Geophys. 40:2–31

Prospero JM, Schmitt R, Cuevas E, Savoie DL, Graustein WC, Turekian KK, Volz-Thomas A, Diaz A, Oltmans SJ, Levy H II (1995) Temporal variability of summer-time ozone and aerosol in the free troposphere over the eastern North Atlantic. Geophys Res Lett 22(21):2925–2928

Rodríguez S, González Y, Cuevas E, Ramos R, Romero PM, Abreu-Afonso J, Redondas A (2009) Atmospheric nanoparticle observations in the low free troposphere during upward orographic flows at Izaña Mountain Observatory. Atmospheric Chem Phys 9:6319–6335. https://doi.org/10.5194/acp-9-6319-2009

Sahoo A, Sarkar S, Singh RP, Kafatos M, Summers ME (2005) Declining trend of total ozone column over the northern parts of India. Int J Remote Sens 26:3433e3440

Santurtun A, Gonzalez-Hidalgo JC, Sanchez-Lorenzo A, Zarrabeitia MT (2015) Surface ozone concentration trends and its relationship with weather types in Spain (2001-2010). Atmos Environ 101:10

Schmitt R, Schreiber B (1998) Effect of long-range transport on atmospheric trace constituents at the baseline station Tenerife (Canary Islands). J Atmos Chem 1:335–351

Singh RP, Sarkar S, Singh A (2002) Effect of El Nin˜o on inter-annual variability of ozone during the period 1978–2000 over the Indian sub-continent and China. Int J Remote Sens 23:2449–2456

Smoydzin L, Fnais M, Lelieveld J (2012) Ozone pollution over the Arabian gulf-role of meteorological conditions, Atmos. Chem Phys Discuss 12:6331–6361

Soler R, Nicolás JF, Caballero S, Yubero E, Crespo J (2016) Depletion of tropospheric ozone associated with mineral dust outbreaks. Environ Sci Pollut Res 23(19):19376–19386

Tang L, Karisson PE, Gu Y, Chen D (2009) Synoptic weather types and long-range transport patterns for ozone precursos during high-ozone events in southern Sweden. Ambio 38:459e464

Torres O, Bhartia PK, Herman JR, Ahmad Z, Gleason K (1998) Derivation of aerosol properties from satellite measurements of backscattered ultraviolet radiation: theoretical basis. J Geophys Res 103:17099–17110

Tsvieli Y, Zangvil A (2005) Synoptic climatological analysis of "wet" and "dry" Red Sea troughs over Israel. Int J Climatol 25:1997–2015. https://doi.org/10.1002/joc.1232

Varotsos C, Cartalis C, Vlamakis A, Keramitsoglou I, Tzanis C (2004) The long-term coupling between column ozone and tropopause properties. J Clim 17:3843–3854

Washington R, Todd M, Middleton MJ, Goudie AS (2003) Dust-storm source areas determined by the Total Ozone Monitoring Spectrometer and surface observations. Ann Assoc Am Geogr 93: 297–313

Zhang Y, Sunwoo Y, Kotamarthi V, Carmichael GR (1994) Photochemical oxidant pro-processes in the presence of dust: an evaluation of the impact of dust on particulate nitrate and processes ozone formation. J Appl Met 33:813–824